

Denoising Distillation Makes Event-Frame Transformers as Accurate Gaze Trackers

Jiading Li¹, Zhiyu Zhu^{1*}, Jinhui Hou¹, Junhui Hou¹, and Jinjian Wu²

¹ City University of Hong Kong, Hong Kong, China

² Xidian University, Xi An, China

Abstract. This paper tackles the problem of passive gaze estimation using both event and frame data. Considering inherently different physiological structures, it's intractable to accurately estimate purely based on a given state. Thus, we reformulate the gaze estimation as the quantification of state transitions from the current state to several prior registered anchor states. Technically, we propose a two-stage learning-based gaze estimation framework to divide the whole gaze estimation process into a coarse-to-fine process of anchor state selection and final gaze location. Moreover, to improve generalization ability, we align a group of local experts with a student network, where a novel denoising distillation algorithm is introduced to utilize denoising diffusion technique to iteratively remove inherent noise of event data. Extensive experiments demonstrate the effectiveness of the proposed method, which greatly surpasses state-of-the-art methods by a large extent of 15%. The code will be publicly available at https://github.com/jdjdli/Denoise_distill_EF_gazetracker.

Keywords: Event-based Vision · Gaze Estimation · Latent Distillation

1 Introduction

Eye gaze tracking represents a critical component of non-verbal communication, serving as an indicator of an individual's underlying intentions and emotional states. The act of establishing eye contact during interpersonal exchanges is a demonstrative signal of attentiveness, interest, and active engagement, contributing to a shared understanding and rapport among interactants.

Over the recent decades, the field of gaze estimation has witnessed an exponential increase in the development of diverse methodologies. These techniques can be generally categorized into three distinct classes: 2D eye feature regression-based approaches [26, 66, 71, 75], 3D model-based eye movement reconstruction algorithms [41], and appearance-based gaze estimation techniques [56]. The first two classifications typically require the utilization of specialized hardware, such as infrared camera systems, to accurately track the eye's position and movement. Conversely, appearance-based methods utilize conventional imaging devices to

* The first two authors contributed equally to this work. Corresponding author. Email: zhiyuzhu2-c@my.cityu.edu.hk.

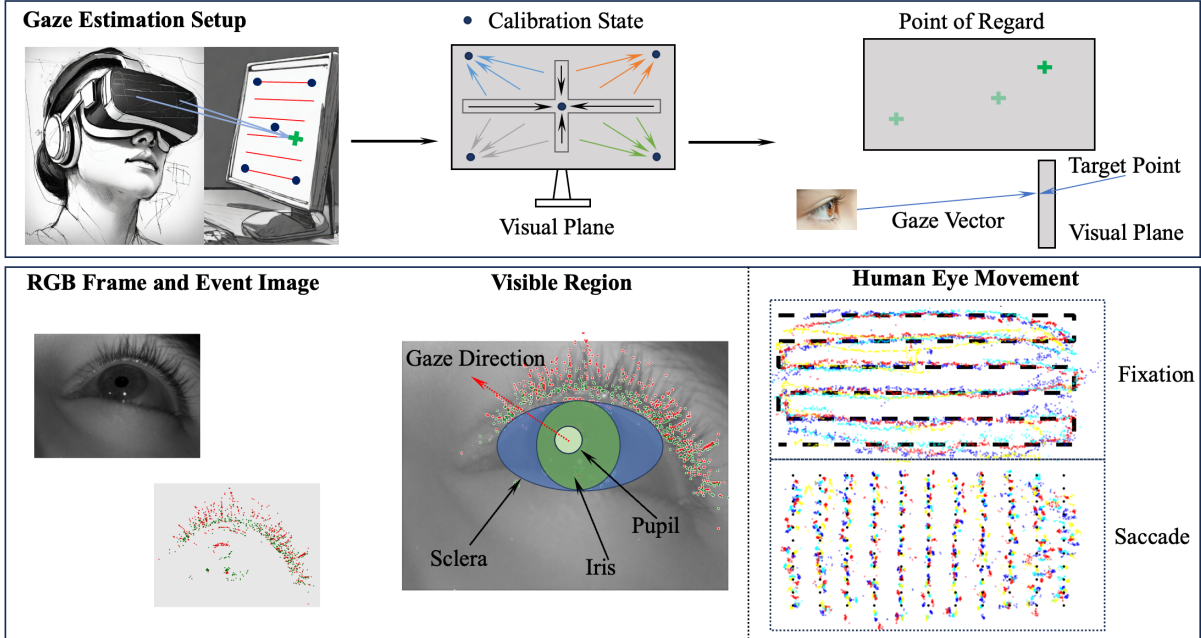


Fig. 1: Top: Overview of our gaze estimation setup. Our framework emphasizes the modeling of gaze shifts from a baseline calibration state, serving as an anchor, to the dynamically acquired state captured during actual use. **Bottom Left:** Our approach ingests input in the form of a frame coupled with corresponding event data, meticulously aligned to highlight the visible region (left). The system is designed to scrutinize the discernible ocular zones (middle), subsequently inferring the directional gaze vector as the output. **Bottom Right:** Beyond the confines of static frame-based gaze estimation, the study of dynamic ocular movements constitutes an additional research trajectory within computer vision.

capture the visual characteristics of the eye and employ machine learning algorithms for gaze direction inference [4, 10, 29, 56]. Despite the accessibility advantages of appearance-based techniques, they often encounter several challenges.

Traditional eye tracking systems that rely on high-speed and high-resolution RGB and optical cameras typically incur substantial costs and energy demands [42, 59]. In contrast, event-based cameras have surged in popularity due to their exceptional temporal resolution, minimal latency, and expansive dynamic range, making them particularly suitable for eye-tracking applications in close-proximity settings [1].

Despite the advantages, event-based sensors provide limited visual information, missing out on color, texture, and comprehensive contextual details that are readily available through conventional RGB imaging [9, 23, 39, 49]. Therefore, the emerging field of cross-modal gaze estimation synthesizes the benefits of both frame and event-based data, presenting an innovative trajectory for bolstering gaze estimation systems [33]. This hybrid approach promises to enhance the robustness and accuracy of gaze tracking by capitalizing on the complementary strengths of both data streams.

In this paper, we delve into the potential of utilizing pre-trained vision Transformers for cross-modal eye tracking, building upon their proven competence in capturing complex spatial-temporal relationships within multi-modal event-frame dataset, as shown in Fig. 1. We present a sophisticated gaze estimation frame-

work that amalgamates the high-temporal-resolution event-driven sensing with the dense spatial information gleaned from frames.

Our system maps the gaze direction with respect to a set of anchor states, employing a dual-phase, coarse-to-fine processing algorithm. In the initial phase, a multi-layer perceptron (MLP) is tasked with the adaptive selection of the most representative template from a predefined library of regional anchor states.

Subsequently, we advocate for the adoption of a distillation of an ensemble of pre-trained local expert networks, thereby enhancing the student’s capacity for accurate gaze prediction across diverse scenarios. Furthermore, we integrate a self-supervised de-noising algorithm into this distillation process to remove potential noise from event data. Our system thus represents a cutting-edge solution in eye tracking, optimizing precision through a harmonized use of event and frames.

In summary, our main contributions are

- we formulate the gaze estimation as a end-to-end prediction of state shifting from selected anchor state;
- we distill multiple pre-trained local expert networks into a more robust student network to combat overfitting in gaze estimation; and
- we propose a self-supervised latent denoising method to mitigate the adverse effects of noise from expert networks to improve the performance of the student network.

2 Related work

In this section, we give a review of event-based vision, eye tracking, event-frame methods, and distillation networks.

Event-based Vision. Neuromorphic event-based cameras, inspired by the Silicon Retina concept [43,47], are key for fast vision tasks due to their quick response and low latency [15,18,36,55]. They support a wide range of applications including object recognition [39,48], navigation [57], pose estimation [51], 3D reconstruction [46], SLAM [14,70], gesture tracking [31], and object tracking [64,69,76,77]. Initially, these cameras used event patterns to detect motion [16,17,37,38] and track simple shapes [11,30]. Later improvements introduced event-driven algorithms [52] and optimization techniques like gradient descent to refine tracking [53]. Algorithms such as mean-shift and Monte Carlo [24,58] have further enhanced tracking by adjusting to changes in the model. For instance, part-based models [58] have segmented subjects into parts, enabling quick and accurate tracking of facial or body movements [34]. However, event data’s sparsity can be problematic in low-contrast settings, and using algorithms designed for dense data in sparse situations may increase computational demands.

Eye Tracking. Progressing from initial camera-based systems of eye tracking that monitored Purkinje images [12,13,35,65,67,73]. Morimoto *et al.* [50] and Duchowski *et al.* [20] provide detailed examinations of these pupil modeling and gaze estimation processes. Contemporary research focuses on deep learning to deduce gaze orientation from complex facial datasets obtained via standard webcams to directly map the

visual characteristics of the eye to gaze coordinates, with Chen *et al.* [8] enhancing accuracy through dilated convolution techniques. Advancing the field, Cheng *et al.* [9] integrates full face and eye region data for more accurate gaze inference and incorporated transformer models to exploit their superior handling of data dependencies. Nonetheless, these advanced models are best for full-face images and not ideal for eye-only cameras, requiring custom-designed networks for accurate data analysis. Also, their effectiveness is limited by the camera’s frame rate, which can affect their real-time accuracy and performance.

Event-frame Methods. Hybrid methods combine the detailed intensity data from standard RGB-based imaging with the rapid detection of intensity changes from asynchronous event streams [3, 22, 32, 74]. Feng *et al.* [22] developed an event-driven eye segmentation algorithm that overcomes the limitations of standard frame rates, maintaining high accuracy despite a lower resolution. Impressively, this model consistently achieved gaze estimation accuracy within a tight error range of $0.1^\circ - 0.5^\circ$. Angelopoulos *et al.* [2] enhanced the temporal resolution of gaze tracking by integrating event cameras close to the eyes. These cameras provided constant updates to the initial pupil location determined by traditional algorithms, allowing for precise adjustments at high temporal resolutions. This approach resulted in gaze estimation accuracy ranging from $0.45^\circ - 1.75^\circ$. However, individual differences can significantly affect the performance of these methods [5, 61].

Distillation Networks. Knowledge distillation [27] is intended for the transference of learned features from a "teacher" model to an efficient variant "student" model. Lopez-Paz *et al.* [40] expanded upon this concept by introducing privileged information, wherein the student model leverages insights from multiple teacher models, each accessing unique and potentially exclusive data sources. Xiang *et al.* [72] advocated for a self-paced knowledge distillation approach, which taps into the collective intelligence of several teacher models to tackle the intricacies of long-tailed distribution problems. Guo *et al.* [25] formulated a collaborative learning framework, akin to a congregation of local experts sharing their knowledge. Post the maturation of these expert networks, the essence of their collective intelligence is distilled into a singular, more generalized student network [6, 60, 62]. This amalgamation of specialized knowledge endows the student network with an enhanced level of accuracy and generalizability, surpassing what could be achieved by an individual model trained on a uniform dataset.

This study conducts an examination of the advantages of fusing conventional intensity frames with dynamic event camera data into a unified network architecture, leveraging pre-existing local expert models. The investigation aims to ascertain if this integration fosters the creation of advanced, resilient, and accurate eye-tracking methods, harnessing the unique benefits of both traditional imaging modalities and innovative event-based sensor inputs.

3 Proposed Method

Method Overview.

Our approach maps gaze direction relative to a series of baseline *registration states* through a dual-phase, coarse-to-fine processing strategy. Generally, as illustrated in Fig. 2, we initially partition the whole dataset into several sub-regions and employ a transformer architecture to train a set of local experts on different regions (see Sec. 3.1), which can obtain several models with relatively high accuracy of gaze estimation in local regions. To diminish the adverse effects of inherent noise from event data on student network performance, we further introduce a latent-denoising distillation method to transfer the knowledge from the set of local experts to a global student network (see Sec. 3.2). In what follows, we will detail our framework.

3.1 Gaze Estimation as State Correlation Modeling

It’s well recognized that gaze direction determination is a multifaceted process intricately linked to the synergistic movements of both the head and the eyes. The kinematic behavior of the head introduces a significant **bias** in gaze estimation algorithms, which cannot be overlooked. Consequently, in lieu of employing conventional methodologies that aim to ascertain the absolute directionality of ocular focus from a singular observational state, our proposed framework pivots towards a more nuanced approach. We advocate for a differential gaze estimation strategy wherein the focus is on modeling the gaze shift relative to an anchor state juxtaposed against the dynamically acquired state. This paradigm shift enables a more robust and accurate gaze inference, accounting for the complexities inherent in head-eye coordination dynamics. Specifically, the proposed gaze estimation pipeline consists of the following three parts:

Event Frame Tokenization. To derive uniform representations of events and frame data, we utilize a convolutional layer and pointnet separately for processing local frame patches and event voxels. With the assistance of convolutional layers, a frame can be effectively embedded into patches, thereby enabling the use of powerful, existing, image-based large-scale pretrained models. Owing to the unique characteristics of event data, we aggregate events within specific time intervals to streamline the asynchronous event flow into a synchronous format, dictated by the exposure duration (which can align with the frames), to form event images. This aggregation is akin to stacking events, a process that mirrors traditional photography exposure. Additionally, we apply voxelization to convert the continuous event stream into a discrete voxel grid. The original event stream, denoted as \mathcal{E} , spans a range defined by height \mathbf{H} , width \mathbf{W} , and time \mathbf{T} . We partition this spatio-temporal domain into a grid of voxels, each with dimensions h', w', t' . Consequently, each voxel encapsulates multiple events, yielding a transformed voxel grid with dimensions $H/h', W/w', T/t'$. To manage this complexity and mitigate the impact of outlier voxels, we prioritize the top \mathbf{K} voxels by the volume of events they contain. Denote the set of selected voxels as $\mathcal{O} = \{o_1, o_2, \dots, o_K\}$. The representation of each selected voxel o_i includes its 3D coordinates (x_i, y_i, t_i) along with the feature descriptor \mathbf{a}_i , formalized as: $o_i = (x_i, y_i, t_i, \mathbf{a}_i)$. Only in a unified form can we proceed with the alignment and fusion of frames and event voxels, culminating in uniform representations of the two modalities of data.

Correlation Modeling. We first construct four embedding representations of two different gaze points: $P_{Est} = (\mathcal{E}_i, \mathcal{O}_i)$, $P_{Temp} = (\mathcal{E}_T, \mathcal{O}_T)$, including the estimation point (measure state point) and the template

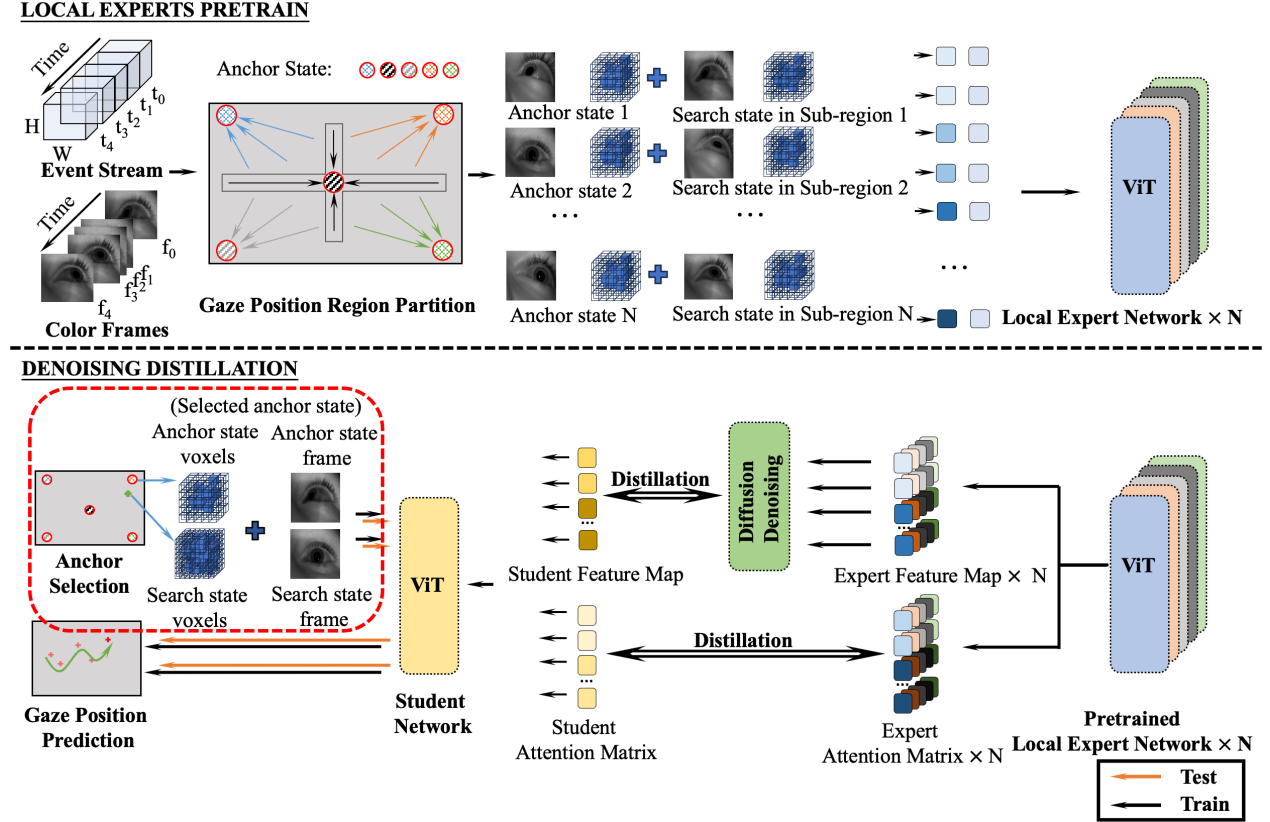


Fig. 2: Illustration of the workflow of the proposed framework, where **Black arrow** (resp. **Orange arrow**) represents the training (resp. testing) pipeline, respectively. **First Stage (Top): Local Experts Pretrain.** We first partition the whole dataset into several sub-regions, wherein each region’s data is trained to cultivate a local expert network. Each expert network is simultaneously fed with the anchor state and a search state and utilize the transformers to explicitly model the correlation between the anchor and states. **Second Stage (Bottom): Denoising Distillation.** A latent-denoising knowledge distillation method is introduced to amalgamate the expertise of these several local expert networks into a singular, comprehensive student network. *Note that the latent denoising and knowledge distillation are utilized in the training phase only. Anchor selection in the red box is illustrated in detail in Fig. 5.*

point (anchor state point). After implementing a sequence of data augmentation techniques, the initial CNN features were derived by embedding these data. Following the initial feature embedding, we utilize the vision transformer to further model the correlation between the current state and the anchor state. This module integrates multi-head self-attention (MSA), an MLP, and layer normalization components. The MSA mechanism is capable of comprehensively capturing the correlation between these two states.

Location Proposal. Initially, the two modality data corresponding (e.g., \mathcal{E}_i and \mathcal{O}_i) to the same state are concatenated subsequent to the embedding process.

This approach is predicated on the premise that data from disparate modalities, yet within the same state, can be effectively aligned and fused. Such integration is advantageous for enhancing the accuracy and assessment velocity of gaze estimation. As shown in Fig. 2, we simultaneously feed anchor and measured states into transformers for correlation modeling. This module is meticulously engineered to effectively distill enhanced different state spatio-temporal features.

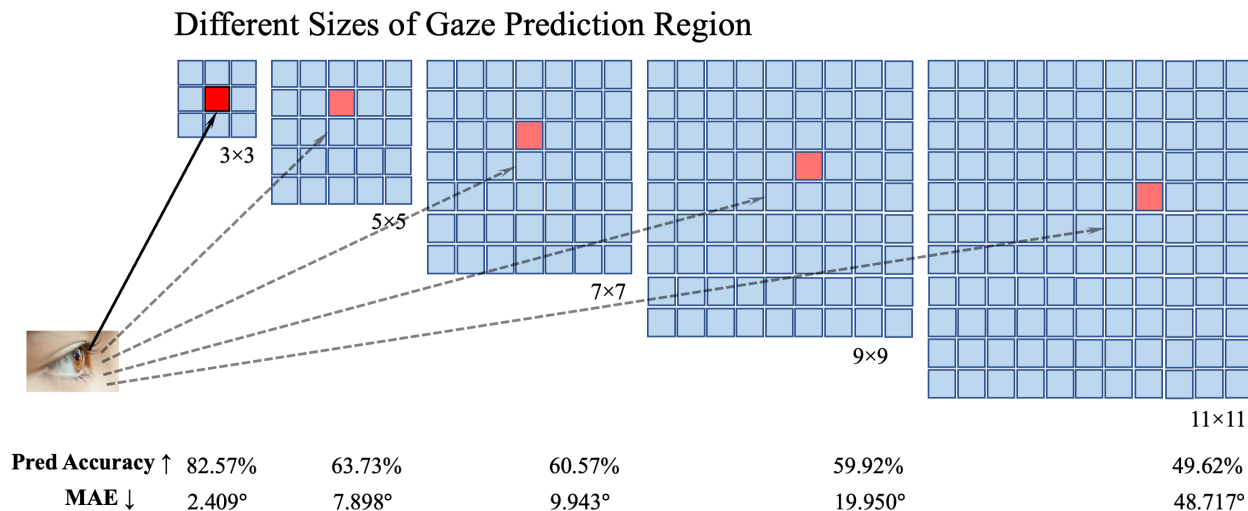


Fig. 3: Comparison of models trained using varying numbers of perceived locations, denoted as $n \times n$. Furthermore, all models share the same architecture and are evaluated on data with perceived regions identical to those in their respective training sets. Evidently, despite progressively expanding the network’s parameters to match the growing size of the predicted region, an incremental increase in the training dataset region leads to a substantial degradation in network performance. This observation suggests the possibility of enhancing network performance on larger regions through the distillation of knowledge from expert models trained on smaller regions. ↑ (resp. ↓) indicates the larger (resp. smaller) the better.

Finally, we flatten them into a feature representation. After that, we utilize one convolutional layer to output the final class label prediction.

3.2 Distillation of Local Experts with Latent Denoising

Instead of engaging in direct end-to-end training of the entire computational architecture, which can precipitate premature convergence to sub-optimal, over-fitted parameters, as evidenced in Fig. 3 and Fig. 4, we combine expertise from local experts into a student network. As illustrated in Fig. 5, the student network consists of two parts: an anchor selection network, which chooses the nearest anchor based on input states, and following a same architecture as expert network that models and locates gaze points.

We employ knowledge distillation to transfer knowledge from several small local expert networks to a student network. Initially, we divide the location map into n sets and train n expert networks (as described in Sec. 3.1), each focusing on a specific location. However, to effectively distill the knowledge from the expert networks into the student network, it is crucial to obtain accurate and representative feature embeddings from the experts. This requires obtaining well-trained network weights from the experts, although achieving an **optimal** weight distribution is often challenging. Additionally, the presence of noise in the measured inputs can disrupt neural network training and negatively impact performance. To alleviate the potential noise for influencing the neural network training, we seek to applying a self-supervised latent denoising neural network for feature maps from experts and then applying knowledge distillation onto student network.

Prior Latent Denoising.

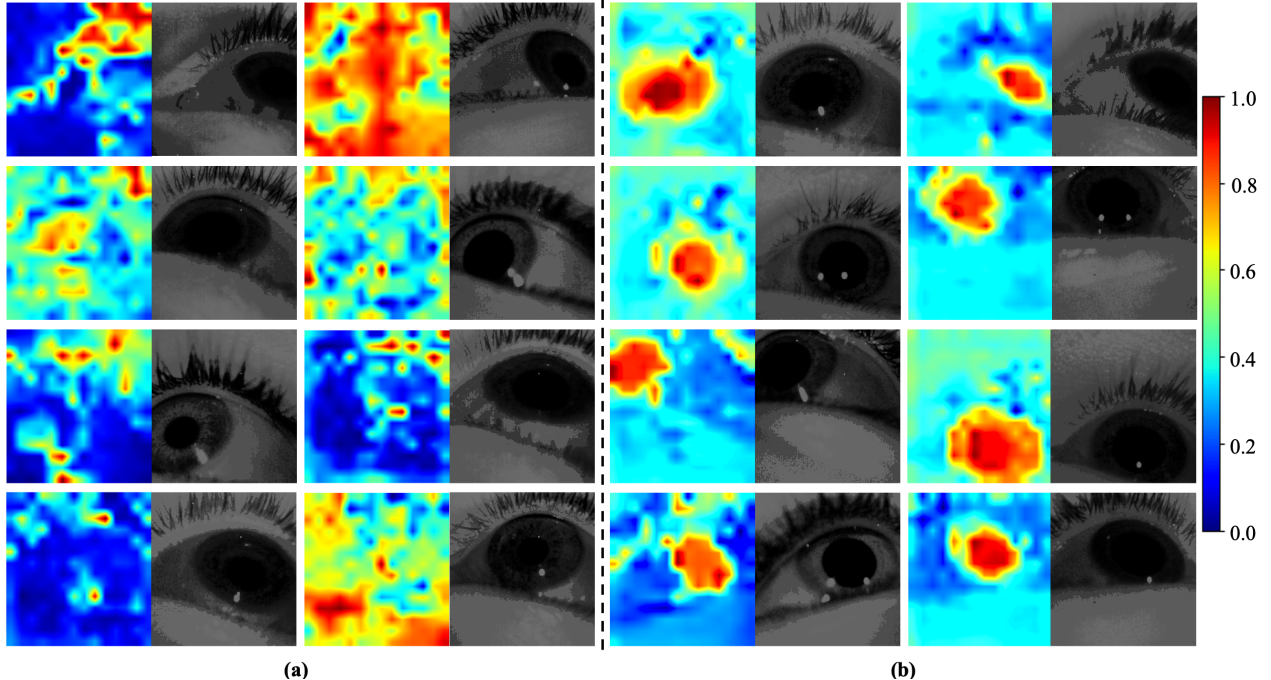


Fig. 4: Visualization of feature maps and ocular region by OpenCV. **(a)** illustrates the outcome of training with a model under a large region, exhibiting pronounced over-fitting, as evidenced by the heatmap, indicating attention dispersion away from the ocular region. **(b)** showcases performance of our model, which make distillation of knowledge from a group of local experts, with a heatmap distinctly concentrated on the ocular region.

To counteract the adverse effects of intrinsic noise in expert feature maps on student network training, we convert the feature map with potential noise into a distribution through sampling. By iteratively sampling the distribution of feature maps and constraining it towards the expected value, we can effectively eliminate the potential noise. Inspired by recent denoising diffusion models [28, 63], we formulate the distribution of the latent feature maps following such a distribution $p(\tilde{x}|x) = \mathcal{N}(\tilde{x}; x, \gamma\mathbf{I})$, where \tilde{x} indicates the measured noised latent, x denotes the corresponding noise-free value of expectation, $\gamma\mathbf{I}$ represents the covariance matrix with the independent assumption. We could then re-parameterize the $\gamma = \sqrt{1 - \gamma'}$ and $x = \sqrt{\gamma'}y$.

Following that, we have $p(\tilde{x}|y) = \mathcal{N}(\tilde{x}; \sqrt{\gamma'}y, \sqrt{1 - \gamma'}\mathbf{I})$. Recalling the intermediate sample of DDPM [28], $x_t = \sqrt{\bar{\alpha}_t}x_0 + \sqrt{1 - \bar{\alpha}_t}x_T$, where $\bar{\alpha}_i = \prod_{j=0}^i \alpha_j$. Thus, the noised latent \tilde{x} could be approximated by certain step result x_i in a diffusion reverse process ($x_T \rightarrow x_0$), where $x_0 = y$ and $\bar{\alpha}_i = \gamma'$. We then introduce a process to drive the distribution of x_i from a sample \tilde{x} by a methodology of adding then removing noise from diffusion models.

The forward process can be simply constructed by adding noise following $x_t = \sqrt{\bar{\alpha}_t}x_{t-1} + \sqrt{1 - \bar{\alpha}_t}\epsilon_t$, where ϵ_t indicates a random noise. Thus, we could train the denoiser as Algorithm 1 to learn the potential noise from noised sample. Please refer to *Supplementary Material* for more details of loss terms in Algorithm 1.

However, our algorithm starts from a noised measurement and iteratively adds then removes noise. Thus, the reverse process of our algorithm is explicitly different with the standard de-noising diffusion model. We should add further delicate analysis of the reverse distribution of the Markov chain, which starts from x_i . We

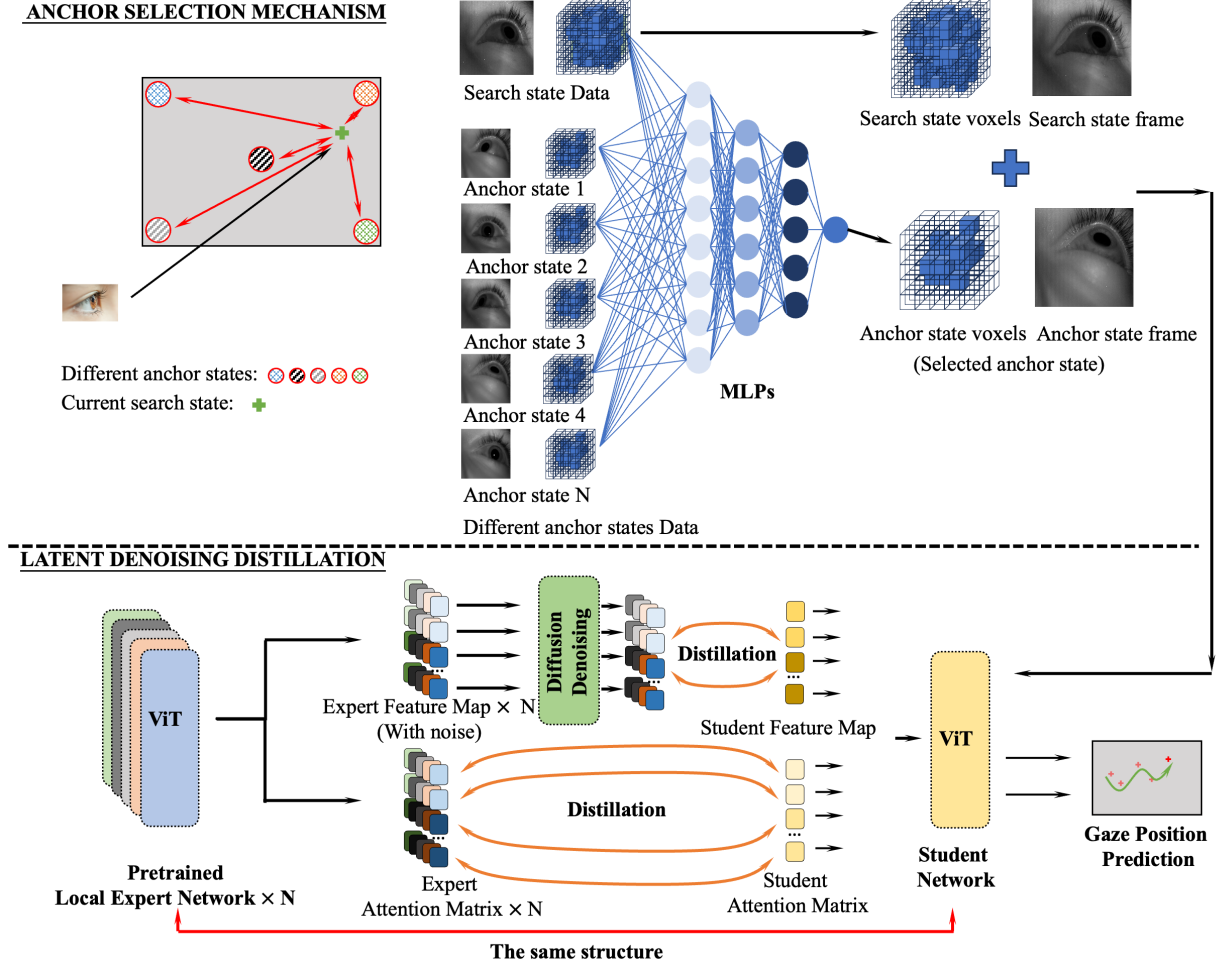


Fig. 5: Our student network initially utilizes an anchor selection mechanism, driven by MLPs, to dynamically identify the most adjacent anchor state in relation to the input state. Subsequently, a latent denoising knowledge distillation is used to transfer knowledge from several small local expert networks to our student network.

begin with one reverse transition process as

$$q(x_{t-1}|x_t, x_i) = \frac{q(x_t|x_{t-1}, x_i)q(x_{t-1}|x_i)}{q(x_t|x_i)}, \quad (1)$$

where x_t indicates the noised sample with inherent noise from collected event data. Then we take an investigation of the term $q(x_{t-1}|x_t, x_i)$.

$$\begin{aligned} q(x_{t-1}|x_t, x_i) &= \frac{q(x_t|x_{t-1}, x_i)q(x_{t-1}|x_i)}{q(x_t|x_i)} \\ &= \frac{\mathcal{N}(x_t, \sqrt{\alpha_t}x_{t-1}, \sqrt{1-\alpha_t}I)\mathcal{N}(x_{t-1}, \sqrt{\frac{\bar{\alpha}_{t-1}}{\bar{\alpha}_i}}x_i, \sqrt{1-\frac{\bar{\alpha}_{t-1}}{\bar{\alpha}_i}}I)}{\mathcal{N}(x_t, \sqrt{\frac{\bar{\alpha}_t}{\bar{\alpha}_i}}x_i, \sqrt{1-\frac{\bar{\alpha}_t}{\bar{\alpha}_i}}I)} \\ &\propto \mathcal{N}(x_{t-1}, \frac{(1-\alpha_t)(\bar{\alpha}_i - \bar{\alpha}_{t-1})}{\bar{\alpha}_i - \bar{\alpha}_t}(\frac{\sqrt{\alpha_t}}{1-\alpha_t}x_t + \frac{\sqrt{\bar{\alpha}_i\bar{\alpha}_{t-1}}}{\bar{\alpha}_i - \bar{\alpha}_{t-1}}x_i), \sqrt{\frac{(1-\alpha_t)(\bar{\alpha}_i - \bar{\alpha}_t)}{\bar{\alpha}_i - \bar{\alpha}_t}}) \end{aligned} \quad (2)$$

Algorithm 1 Training Denoiser

```

1: Repeat
2:  $\mathbf{x}_i \sim q(\mathbf{x}_i)$ 
3:  $t \sim \text{Uniform}(\{i, i+1, \dots, T\})$ 
4:  $\epsilon \sim \mathcal{N}(0, \mathbf{I})$ 
5:  $i \sim \mathcal{U}(27, 32)$ 
6: Take gradient descent step on
7:    $\delta = \epsilon - \epsilon_\theta(\sqrt{\frac{\bar{\alpha}_t}{\bar{\alpha}_i}}x_i + \sqrt{1 - \frac{\bar{\alpha}_t}{\bar{\alpha}_i}}\epsilon, t)$ 
8:    $\nabla_\theta \|\sum \delta\|^2 + \|\sigma(\delta) - \sqrt{2}\|^2$ 
9: Until converged

```

Algorithm 2 Reverse process

```

1:  $\epsilon \sim \mathcal{N}(0, \mathbf{I})$ 
2:  $x_{T'} = \sqrt{\frac{\bar{\alpha}_{T'}}{\bar{\alpha}_i}}x_i + \sqrt{1 - \frac{\bar{\alpha}_{T'}}{\bar{\alpha}_i}}\epsilon$ 
3: For  $t = T', \dots, i$  do
4:    $\mathbf{z} \sim \mathcal{N}(0, \mathbf{I})$  if  $t > i$ , else  $\mathbf{z} = 0$ 
5:    $\sigma_t = \sqrt{\frac{\hat{\beta}_t(\bar{\alpha}_i - \bar{\alpha}_{t-1})}{\bar{\alpha}_i - \bar{\alpha}_t}}$ 
6:    $x_{t-1} = \frac{1}{\sqrt{\alpha_t}}(x_t - \frac{(1-\alpha_t)\sqrt{\bar{\alpha}_i}}{\sqrt{\bar{\alpha}_i - \bar{\alpha}_t}}\epsilon_\theta(x_t, t)) + \sigma_t \mathbf{z}$ 
7: End for
8: Return  $\mathbf{X}_i$ 

```

Moreover, with $\hat{\beta}_t = 1 - \alpha_t$, we have,

$$q(x_{t-1}|x_t, x_i) \propto \mathcal{N}(x_{t-1}, \frac{\hat{\beta}_t(\bar{\alpha}_i - \bar{\alpha}_{t-1})}{\bar{\alpha}_i - \bar{\alpha}_t}(\frac{\sqrt{\alpha_t}}{\hat{\beta}_t}x_t + \frac{\sqrt{\bar{\alpha}_i \bar{\alpha}_{t-1}}}{\bar{\alpha}_i - \bar{\alpha}_{t-1}}x_i), \sqrt{\frac{\hat{\beta}_t(\bar{\alpha}_i - \bar{\alpha}_{t-1})}{\bar{\alpha}_i - \bar{\alpha}_t}}) \quad (3)$$

However, such a noise level indicated by i is quite hard to derive. Thus, during the training phase, we relax $\bar{\alpha}_i$ to a certain range of $i \in [27, 32]$. Note that through aforementioned reverse process, we derive the distribution of x_i from it's certain measurement by iteratively sample $x_{t-1}, t = T', \dots, i$, as Eq. (3), which is detailedly illustrated in Algorithm 2. Although we do not explicitly remove the noise from the data, we expect during the training process, the variable x would be converged to the noise-free expectation x_0 as

$$x = \underset{x}{\operatorname{argmin}} \sum \mathcal{L}_d(x, x_i), \mathcal{L}_d(x, x_i) = \|x - \frac{x_i}{\sqrt{\bar{\alpha}_i}}\|_2^2 = \|x - x_0 + \sqrt{\frac{1 - \bar{\alpha}_i}{\bar{\alpha}_i}}\epsilon'\|_2^2, \quad (4)$$

where ϵ' is a standard Gaussian noise. Thus, there is only one optimal solution, i.e., $x = x_0$.

3.3 Training Objective

We train our two-stage gaze estimation framework in a two-stage training manner. In the first stage, we use gaze labels and apply eye loss \mathcal{L}_e to train the local experts, which ensures that our local experts maintain optimal performance. We distill these local experts into a student network in the second stage. Noted that in the second training stage, we add more substantial supervision for the entire dataset training, allowing our network to learn better. The loss \mathcal{L}_e is kept to ensure stable performance as hard loss. Meanwhile, we use the attention metrics of local experts and apply a soft loss \mathcal{L}_s to guide the learning of the student network. Finally, a feature map loss \mathcal{L}_d is used to guide the gaze estimation. The loss of the whole model is the weighting of these three losses:

$$\mathcal{L} = \alpha \cdot \mathcal{L}_e + \beta \cdot \mathcal{L}_s + \gamma \cdot \mathcal{L}_d, \quad (5)$$

where α , β , and γ are corresponding weight for balancing different loss terms.

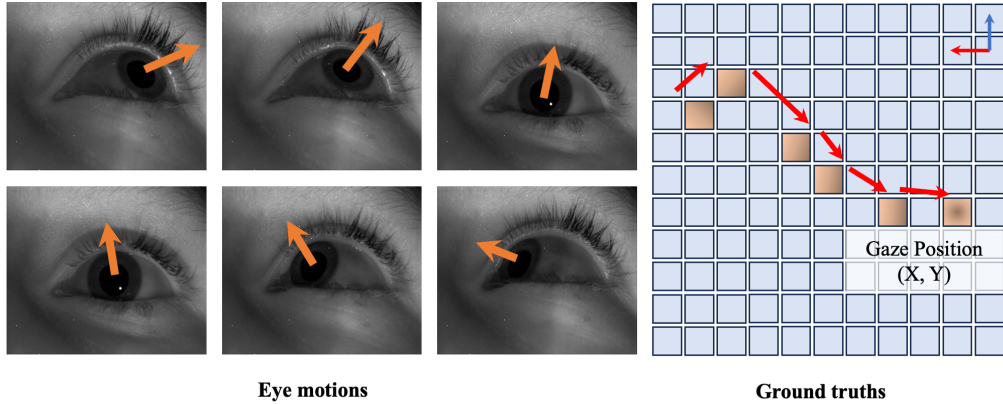


Fig. 6: Illustrative depictions of ocular motion trajectories and the associated gaze coordinates on the visual field.

4 Experiment

4.1 Experimental Settings

Dataset. We utilized a hybrid Event IR-based near-eye gaze tracking dataset [2] to evaluate our proposed system. Here is a brief introduction to this dataset.

The dataset encompasses biometric recordings from 24 subjects, partitioned into two distinct experimental conditions tailored to elicit divergent oculomotor responses: stochastic saccadic movements and controlled smooth pursuit tracking. The visual stimulus, a 40×40 -pixel luminous green fixation cross, is superimposed on a circular background with a diameter of 20 pixels, set against a uniform black field to minimize peripheral visual cues. The display apparatus is configured to encompass a visual field of view (FoV) of $64^\circ \times 96^\circ$.

During the first experimental paradigm, subjects were instructed to direct their gaze towards the stimulus, which materialized at random within a grid matrix of 121 discrete points (an 11×11 grid pattern projected onto the display medium), with each point being presented for a temporal duration of 1.5 seconds. This sequence of locations was uniformly randomized and remained consistent across all participants. Some sample images are shown in Fig. 6.

Implementation details. We configure the mini-batch size to 80 and adopt the AdamW optimization algorithm due to its efficacy in handling sparse gradients and incorporating weight decay for regularization. We initiate the training with a learning rate of 0.0001, which is methodically attenuated following a cosine annealing schedule, descending to a factor of 0.1 of the original learning rate at its nadir. The first stage of training spans across 350 epochs to ensure the local expert network adequately learns the intricate patterns within the data.

In the subsequent stage, the five local expert networks are distilled into the student network, leveraging the AdamW optimizer once again. This phase is conducted with a reduced learning rate of 0.00001 and a momentum coefficient of 0.9, extending over 500 epochs. Due to the computationally intensive nature of

Table 1: Quantitative results of different methods. \downarrow (resp. \uparrow) indicates the smaller (resp. larger), the better.

Method	S-T GE [54]	Dilated-Net [8]	EventGT [75]	HE-Tracker [7]	Ours
MAE \downarrow	7.650°	4.020°	3.000°	4.170°	1.928°
Accuracy \uparrow	61.88%	66.63%	72.06%	72.87%	87.67%
Time (ms)	288.34	562.03	—	20.65	191.25

knowledge distillation, the mini-batch size is adjusted to 4 to accommodate the increased model complexity and ensure stable convergence. Code is implemented using Pytorch and trained with RTX3090 GPUs.

Methods under comparison. We experimentally compared the following four methods:

- **S-T GE** [54] leverages temporal sequences of eye images to enhance the accuracy of an end-to-end appearance-based deep-learning model for gaze estimation.
- **Dilated-Net** [8] integrates dilated convolutional layers to enhance feature extraction for gaze estimation.
- **EventGT** [75] achieves an equilibrium of computational efficiency and accuracy—a key consideration for real-time gaze tracking.
- **HE-Tracker** [7] employs a sophisticated pipeline that commences with the E-Tracker’s encoding of eye imagery.

Metrics. Following previous works [7], we employed the Mean Angle Error (MAE) to evaluate the performance quantitatively, computed as

$$\text{MAE} = \frac{1}{N} \sum_{i=1}^N \arccos \frac{\langle \vec{p}_i, \vec{t}_i \rangle}{\|\vec{p}_i\| \|\vec{t}_i\|} \quad (6)$$

where N is the number of samples in the dataset, \vec{p}_i is the predicted gaze vector for the i -th sample, \vec{t}_i is the corresponding ground truth vector, and $\langle \cdot, \cdot \rangle$ computes the inner product of two input vectors. Moreover, we calculate the prediction accuracy.

4.2 Comparison with State-of-the-Art Methods

We conducted a comparative analysis of the inference outcomes across various model architectures within the specialized domain of gaze estimation. The quantitative results of this assessment are systematically presented in Table 1. The empirical data gleaned from these comparisons unequivocally corroborate the effectiveness of our proposed framework, as evidenced by its superior performance metrics in gaze estimation tasks that nearly 50% improvement about the MAE and 15% improvement of tracking accuracy.

4.3 Ablation Study

Data Modality. We commence our investigation by scrutinizing the impact of various data modalities on the efficacy of the model’s performance. Employing exclusively frames for gaze estimation engendered a

Table 2: Gaze estimation performance across various data modalities and denoising, where “F” indicates the frame and “E” represents the event.

Metric	F	E	Ours (F+E)	Ours w/o Denoising
MAE ↓	40.161°	—	1.928°	3.472°
Accuracy ↑	53.00%	1.45%	87.67%	84.64%

prognostication characterized by an angular error of 40.16°, which is much higher than dual-model baseline, only 1.93°. In contrast, the exclusive utilization of event-based data yielded a prediction with a very low prediction accuracy of 1.45%. These outcomes are juxtaposed against our established baseline model, with the corresponding results meticulously enumerated in Table 2. The observed decrement in performance metrics underscores the quintessential role of amalgamating frames with event-based data for enhanced accuracy. Although both frames and event-based sensor data demonstrate an associative relationship with the directional vector of gaze, their isolated use is sub-optimal for the precise delineation of gaze coordinates. The amalgamation of frames with event data culminated in the most accurate gaze prediction. This indicates that the synergy of event-based features with frame data can substantially bolster the model’s performance, particularly as the quantity of motion-related information escalates.

Latent Denoising. We also conducted experiments to validate the effectiveness of latent denoising. As shown in Table. 2, with the latent denoising our method achieves nearly 3% improvements of accuracy and 44.5% improvements of MAE, showcasing the potential of the proposed denoising distillation strategy. Note that the latent denoising is utilized in the training phase only before distillation, and the total number of parameters of student network remains unchanged.

Anchor State. Subsequent to our initial inquiry, we conducted a series of ablation studies to ascertain the imperativeness of anchor state selection on the performance of our gaze estimation model, where anchor state is same with the number of local expert networks. In the absence of any anchor state integration, our model yielded gaze estimations with an angular error of 32.00°. In marked divergence, the integration of a single anchor state precipitated a substantial mitigation of angular error to 15.19°, thereby highlighting the fundamental importance of anchor in the enhancement of gaze prediction fidelity. A progressive augmentation in the number of anchor states correlated with a concomitant improvement in estimation precision, demonstrably evidencing the anchor state’s critical contribution to the model’s predictive prowess. These empirical findings are concisely encapsulated in Fig. 7 (a).

Weight of Feature Map Loss. Within our model, a feature map loss \mathcal{L}_d is employed to the guidance of the learning algorithm. We investigated how the distillation weight affect the learning process. Note that the gradient from MSE loss (feature distillation) is typically smaller than KL-divergence (task loss), to balance those different terms, we give a large factor for distillation loss \mathcal{L}_d . As shown in Fig. 7 (b), it can be seen

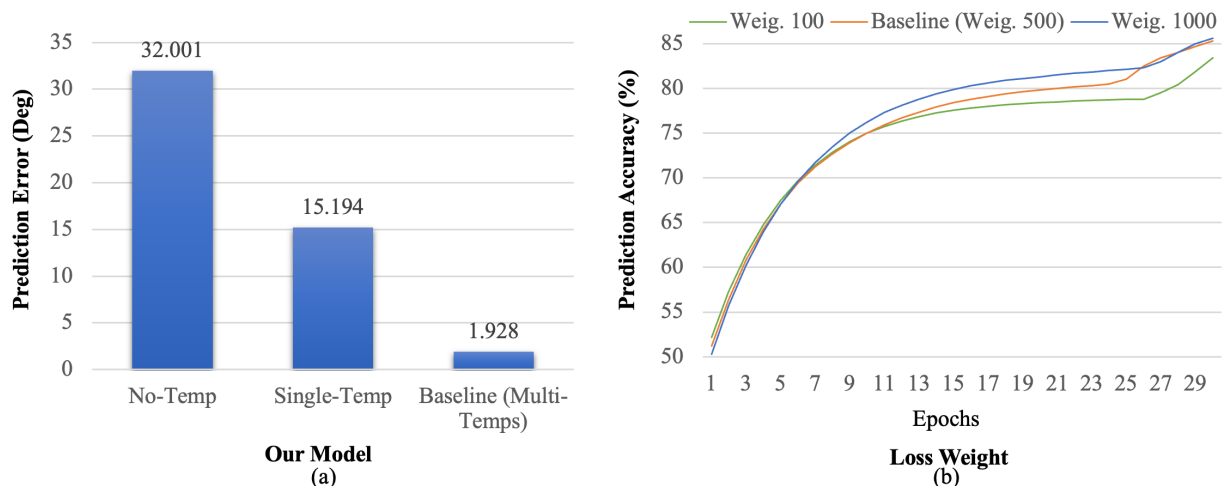


Fig. 7: (a) Performance across different numbers of calibration states. (b) Comparative analysis of model performance subject to varying weights assigned to feature map loss.

Table 3: Gaze estimation performance across various gradient accumulation steps.

Metric	4 Steps	8 Steps	Baseline(16 Steps)
MAE ↓	3.987°	2.684°	1.928°
Accuracy ↑	82.01%	85.48%	87.67%

that the weight of distillation loss is quite large. Such an increment is imperative to augment the network’s learning capacity, thereby enhancing the precision of gaze estimation.

Gradient Accumulation. As shown in Eq. (4), we expect the network could learn the noise-free samples from multiple noised measurement. Thus, enlarging the batchsize is necessary step to make the solution value of Eq. (4) converge to expectation. Our ablation study also investigated the impact of varying gradient accumulation, including 4, 8, and 16 steps. The empirical outcomes are shown in Table 3. The results indicate a positive correlation between the augmentation of gradient accumulation steps and the enhancement in the accuracy of gaze estimation. Concomitantly, there is an observable decrease in the MAE. It indicates that without enough batchsize the noised sample may potentially reduce the the model’s predictive capabilities, since the gradients of Eq. (4) in small batch may lead to deteriorated model weight distributions. The results demonstrate that this approach inherently provides a correct gradient descent direction, effectively reducing the overfitting.

5 Conclusion and Discussion

We have presented a novel coarse-to-fine dual-stage model for gaze estimation that leverages frame data with event data, utilizing anchor states to enhance precision. Technically, we employed transformer networks and knowledge distillation to effectively merge the unique attributes of frame and event data. Our extensive

experiments confirm the model’s capability to tackle challenges in multimodal data fusion, such as reducing overfitting tendencies linked to heavy feature dependence. Our approach achieves reliable gaze estimation, maintaining angular error below 2° , which outperforms various contemporary state-of-the-art gaze estimation methods, setting a new standard for this intricate task.

Despite the substantial superiority of the proposed method compared to state-of-the-art approaches, it is imperative to address additional considerations for further advancement. It is necessary to focus on the development of lightweight neural networks to optimize the inference process, which can be accomplished through techniques like distillation or neural network pruning. Furthermore, there is scope for enhancing accuracy at the retina-level (below 1°), akin to the exceptional capabilities demonstrated by APPLE Vision Pro and HTC Vive.

References

1. Angelopoulos, A.N., Martel, J.N., Kohli, A.P., Conradt, J., Wetzstein, G.: Event-based near-eye gaze tracking beyond 10,000 hz. *IEEE Transactions on Visualization and Computer Graphics* **27**(5), 2577–2586 (2021). <https://doi.org/10.1109/TVCG.2021.3067784> **2**
2. Angelopoulos, A.N., Martel, J.N., Kohli, A.P., Conradt, J., Wetzstein, G.: Event based, near eye gaze tracking beyond 10,000 hz. *arXiv preprint arXiv:2004.03577* (2020) **4, 11, 21**
3. Ansari, M.F., Kasproski, P., Peer, P.: Person-specific gaze estimation from low-quality webcam images. *Sensors* **23**(8) (2023). <https://doi.org/10.3390/s23084138>, <https://www.mdpi.com/1424-8220/23/8/4138> **4**
4. Baluja, S., Pomerleau, D.: Non-intrusive gaze tracking using artificial neural networks. In: Cowan, J., Tesauro, G., Alspector, J. (eds.) *Advances in Neural Information Processing Systems*. vol. 6. Morgan-Kaufmann (1993), https://proceedings.neurips.cc/paper_files/paper/1993/file/19b650660b253761af189682e03501dd-Paper.pdf **2**
5. Bao, J., Liu, B., Yu, J.: An individual-difference-aware model for cross-person gaze estimation. *IEEE Transactions on Image Processing* **31**, 3322–3333 (2022). <https://doi.org/10.1109/TIP.2022.3171416> **4**
6. Bicsi, L., Alexe, B., Ionescu, R.T., Leordeanu, M.: Jedi: Joint expert distillation in a semi-supervised multi-dataset student-teacher scenario for video action recognition (2023) **4**
7. Chen, L., Li, Y., Bai, X., Wang, X., Hu, Y., Song, M., Xie, L., Yan, Y., Yin, E.: Real-time gaze tracking with head-eye coordination for head-mounted displays. In: *2022 IEEE International Symposium on Mixed and Augmented Reality (ISMAR)*. pp. 82–91 (2022). <https://doi.org/10.1109/ISMAR55827.2022.00022> **12, 24**
8. Chen, Z., Shi, B.E.: Appearance-based gaze estimation using dilated-convolutions (2019) **4, 12, 24**
9. Cheng, Y., Lu, F.: Gaze estimation using transformer. In: *2022 26th International Conference on Pattern Recognition (ICPR)*. pp. 3341–3347 (2022). <https://doi.org/10.1109/ICPR56361.2022.9956687> **2, 4**
10. Cheng, Y., Lu, F.: Dvgaze: Dual-view gaze estimation. In: *2023 IEEE/CVF International Conference on Computer Vision (ICCV)*. pp. 20575–20584 (2023). <https://doi.org/10.1109/ICCV51070.2023.01886> **2**
11. Conradt, J., Cook, M., Berner, R., Lichtsteiner, P., Douglas, R., Delbruck, T.: A pencil balancing robot using a pair of aer dynamic vision sensors. pp. 781 – 784 (06 2009). <https://doi.org/10.1109/ISCAS.2009.5117867> **3**
12. Cornsweet, T.N., Crane, H.D.: Accurate two-dimensional eye tracker using first and fourth purkinje images. *JOSA* **63**(8), 921–928 (1973) **3**

13. Crane, H.D., Steele, C.M.: Generation-v dual-purkinje-image eyetracker. *Applied optics* **24**(4), 527–537 (1985) [3](#)
14. Davison, A.J., Reid, I.D., Molton, N.D., Stasse, O.: Monoslam: Real-time single camera slam. *IEEE Transactions on Pattern Analysis and Machine Intelligence* **29**(6), 1052–1067 (2007). <https://doi.org/10.1109/TPAMI.2007.1049> [3](#)
15. Delbruck, T.: Silicon retina with correlation-based, velocity-tuned pixels. *IEEE Transactions on Neural Networks* **4**(3), 529–541 (1993). <https://doi.org/10.1109/72.217194> [3](#)
16. Delbruck, T., Lichtsteiner, P.: Fast sensory motor control based on event-based hybrid neuromorphic-procedural system. In: 2007 IEEE International Symposium on Circuits and Systems (ISCAS). pp. 845–848 (2007). <https://doi.org/10.1109/ISCAS.2007.378038> [3](#)
17. Delbruck, T., Lang, M.: Robotic goalie with 3 ms reaction time at 4% cpu load using event-based dynamic vision sensor. *Frontiers in Neuroscience* **7** (2013). <https://doi.org/10.3389/fnins.2013.00223>, <https://www.frontiersin.org/journals/neuroscience/articles/10.3389/fnins.2013.00223> [3](#)
18. Delbrück, T., Linares-Barranco, B., Culurciello, E., Posch, C.: Activity-driven, event-based vision sensors. In: 2010 IEEE International Symposium on Circuits and Systems - Proceedings (2010), 2010 IEEE International Symposium on Circuits and Systems - ISCAS 2010 ; Conference date: 30-05-2010 Through 02-06-2010 [3](#)
19. Duchowski, A.T., Krejtz, K., Volonte, M., Hughes, C.J., Brescia-Zapata, M., Orero, P.: 3d gaze in virtual reality: Vergence, calibration, event detection. *Procedia Computer Science* **207**, 1641–1648 (2022). <https://doi.org/https://doi.org/10.1016/j.procs.2022.09.221>, <https://www.sciencedirect.com/science/article/pii/S187705092201105X>, knowledge-Based and Intelligent Information & Engineering Systems: Proceedings of the 26th International Conference KES2022 [23](#)
20. Duchowski, T.A.: *Eye tracking: methodology theory and practice*. Springer (2017) [3](#)
21. Elmadjian, C., Shukla, P., Tula, A.D., Morimoto, C.H.: 3d gaze estimation in the scene volume with a head-mounted eye tracker. In: *Proceedings of the Workshop on Communication by Gaze Interaction. COGAIN '18, Association for Computing Machinery, New York, NY, USA* (2018). <https://doi.org/10.1145/3206343.3206351>, <https://doi.org/10.1145/3206343.3206351> [23](#)
22. Feng, Y., Goulding-Hotta, N., Khan, A., Reyserhove, H., Zhu, Y.: Real-time gaze tracking with event-driven eye segmentation. In: 2022 IEEE Conference on Virtual Reality and 3D User Interfaces (VR). pp. 399–408. IEEE (2022) [4](#)
23. Gehrig, D., Rebecq, H., Gallego, G., Scaramuzza, D.: Asynchronous, Photometric Feature Tracking Using Events and Frames, p. 766–781. Springer International Publishing (2018). https://doi.org/10.1007/978-3-030-01258-8_46, http://dx.doi.org/10.1007/978-3-030-01258-8_46 [2](#)
24. Glover, A., Bartolozzi, C.: Robust visual tracking with a freely-moving event camera. In: 2017 IEEE/RSJ International Conference on Intelligent Robots and Systems (IROS). pp. 3769–3776 (2017). <https://doi.org/10.1109/IROS.2017.8206226> [3](#)
25. Guo, Q., Wang, X., Wu, Y., Yu, Z., Liang, D., Hu, X., Luo, P.: Online knowledge distillation via collaborative learning. In: *Proceedings of the IEEE/CVF Conference on Computer Vision and Pattern Recognition (CVPR)* (June 2020) [4](#)
26. Hennessey, C., Nouredin, B., Lawrence, P.: A single camera eye-gaze tracking system with free head motion. In: *Proceedings of the 2006 Symposium on Eye Tracking Research & Applications*. p. 87–94. ETRA '06, Association

- for Computing Machinery, New York, NY, USA (2006). <https://doi.org/10.1145/1117309.1117349>, <https://doi.org/10.1145/1117309.1117349> 1
27. Hinton, G., Vinyals, O., Dean, J.: Distilling the knowledge in a neural network (2015) 4
 28. Ho, J., Jain, A., Abbeel, P.: Denoising diffusion probabilistic models. *Advances in neural information processing systems* **33**, 6840–6851 (2020) 8
 29. Kraflka, K., Khosla, A., Kellnhofer, P., Kannan, H., Bhandarkar, S., Matusik, W., Torralba, A.: Eye tracking for everyone (2016) 2
 30. Lagorce, X., Meyer, C., Ieng, S.H., Filliat, D., Benosman, R.: Asynchronous event-based multikernel algorithm for high-speed visual features tracking. *IEEE transactions on neural networks and learning systems* **26** (09 2014). <https://doi.org/10.1109/TNNLS.2014.2352401> 3
 31. Lee, J., Park, P., Shin, C.W., Ryu, H., Kang, B.C., Delbruck, T.: Touchless hand gesture ui with instantaneous responses. pp. 1957–1960 (09 2012). <https://doi.org/10.1109/ICIP.2012.6467270> 3
 32. Lei, Y., He, S., Khamis, M., Ye, J.: An end-to-end review of gaze estimation and its interactive applications on handheld mobile devices. *ACM Comput. Surv.* **56**(2) (sep 2023). <https://doi.org/10.1145/3606947>, <https://doi.org/10.1145/3606947> 4
 33. Leutenegger, S., Lynen, S., Bosse, M., Siegwart, R., Furgale, P.: Keyframe-based visual-inertial odometry using nonlinear optimization. *The International Journal of Robotics Research* **34**(3), 314–334 (2015). <https://doi.org/10.1177/0278364914554813>, <https://doi.org/10.1177/0278364914554813> 2
 34. Li, N., Chang, M., Raychowdhury, A.: E-gaze: Gaze estimation with event camera. *IEEE Transactions on Pattern Analysis and Machine Intelligence* pp. 1–16 (2024). <https://doi.org/10.1109/TPAMI.2024.3359606> 3
 35. Li, Y., Wang, S., Ding, X.: Eye/eyes tracking based on a unified deformable template and particle filtering. *Pattern Recognition Letters* **31**(11), 1377–1387 (2010). <https://doi.org/https://doi.org/10.1016/j.patrec.2010.02.013>, <https://www.sciencedirect.com/science/article/pii/S016786551000070X> 3
 36. Lichtsteiner, P., Posch, C., Delbruck, T.: A 128×128 120 db 15μ s latency asynchronous temporal contrast vision sensor. *Solid-State Circuits, IEEE Journal of* **43**, 566 – 576 (03 2008). <https://doi.org/10.1109/JSSC.2007.914337> 3
 37. Litzenberger, M., Kohn, B., Belbachir, A., Donath, N., Gritsch, G., Garn, H., Posch, C., Schraml, S.: Estimation of vehicle speed based on asynchronous data from a silicon retina optical sensor. In: 2006 IEEE Intelligent Transportation Systems Conference. pp. 653–658 (2006). <https://doi.org/10.1109/ITSC.2006.1706816> 3
 38. Litzenberger, M., Posch, C., Bauer, D., Belbachir, A., Schon, P., Kohn, B., Garn, H.: Embedded vision system for real-time object tracking using an asynchronous transient vision sensor. In: 2006 IEEE 12th Digital Signal Processing Workshop & 4th IEEE Signal Processing Education Workshop. pp. 173–178 (2006). <https://doi.org/10.1109/DSPWS.2006.265448> 3
 39. Liu, H., Moeys, D.P., Das, G., Neil, D., Liu, S.C., Delbrück, T.: Combined frame- and event-based detection and tracking. In: 2016 IEEE International Symposium on Circuits and Systems (ISCAS). pp. 2511–2514 (2016). <https://doi.org/10.1109/ISCAS.2016.7539103> 2, 3
 40. Lopez-Paz, D., Bottou, L., Schölkopf, B., Vapnik, V.: Unifying distillation and privileged information (2016) 4
 41. Lu, C., Chakravarthula, P., Liu, K., Liu, X., Li, S., Fuchs, H.: Neural 3d gaze: 3d pupil localization and gaze tracking based on anatomical eye model and neural refraction correction. In: 2022 IEEE International Symposium

- on Mixed and Augmented Reality (ISMAR). pp. 375–383 (2022). <https://doi.org/10.1109/ISMAR55827.2022.00053> 1
42. Lystbæk, M.N., Pfeuffer, K., Grønbaek, J.E.S., Gellersen, H.: Exploring gaze for assisting freehand selection-based text entry in ar. *Proc. ACM Hum.-Comput. Interact.* **6**(ETRA) (may 2022). <https://doi.org/10.1145/3530882>, <https://doi.org/10.1145/3530882> 2
 43. Mahowald, M.A.: An analog visi system for stereoscopic vision (1994), <https://api.semanticscholar.org/CorpusID:60778343> 3
 44. Man, Y., Zhao, X., Zhang, K.: 3D gaze estimation based on facial feature tracking. In: Zhu, Z. (ed.) *International Conference on Graphic and Image Processing (ICGIP 2012)*. vol. 8768, p. 87681N. International Society for Optics and Photonics, SPIE (2013). <https://doi.org/10.1117/12.2010781>, <https://doi.org/10.1117/12.2010781> 23
 45. Mansouryar, M., Steil, J., Sugano, Y., Bulling, A.: 3d gaze estimation from 2d pupil positions on monocular head-mounted eye trackers. In: *Proceedings of the Ninth Biennial ACM Symposium on Eye Tracking Research & Applications. ETRA '16, ACM* (Mar 2016). <https://doi.org/10.1145/2857491.2857530>, <http://dx.doi.org/10.1145/2857491.2857530> 23
 46. Martel, J., Muller, J., Conradt, J., Sandamirskaya, Y.: An active approach to solving the stereo matching problem using event-based sensors. pp. 1–5 (05 2018). <https://doi.org/10.1109/ISCAS.2018.8351411> 3
 47. Mead, C.A., Mahowald, M.: A silicon model of early visual processing. *Neural Networks* **1**(1), 91–97 (1988). [https://doi.org/https://doi.org/10.1016/0893-6080\(88\)90024-X](https://doi.org/https://doi.org/10.1016/0893-6080(88)90024-X), <https://www.sciencedirect.com/science/article/pii/089360808890024X> 3
 48. Mitrokhin, A., Fermuller, C., Parameshwara, C., Aloimonos, Y.: Event-based moving object detection and tracking. In: *2018 IEEE/RSJ International Conference on Intelligent Robots and Systems (IROS)*. IEEE (Oct 2018). <https://doi.org/10.1109/iros.2018.8593805>, <http://dx.doi.org/10.1109/IROS.2018.8593805> 3
 49. Mokatren, M., Kuflik, T., Shimshoni, I.: 3d gaze estimation using rgb-ir cameras. *Sensors* **23**(1) (2023). <https://doi.org/10.3390/s23010381>, <https://www.mdpi.com/1424-8220/23/1/381> 2
 50. Morimoto, C.H., Mimica, M.R.: Eye gaze tracking techniques for interactive applications. *Computer vision and image understanding* **98**(1), 4–24 (2005) 3
 51. Mueggler, E., Rebecq, H., Gallego, G., Delbruck, T., Scaramuzza, D.: The event-camera dataset and simulator: Event-based data for pose estimation, visual odometry, and slam. *The International Journal of Robotics Research* **36**(2), 142–149 (Feb 2017). <https://doi.org/10.1177/0278364917691115>, <http://dx.doi.org/10.1177/0278364917691115> 3
 52. Ni, Z., Bolopion, A., Agnus, J., Benosman, R., Regnier, S.: Asynchronous event-based visual shape tracking for stable haptic feedback in microrobotics. *IEEE Transactions on Robotics* **28**(5), 1081–1089 (2012). <https://doi.org/10.1109/TR0.2012.2198930> 3
 53. Ni, Z., Ieng, S.H., Posch, C., Régnier, S., Benosman, R.: Visual Tracking Using Neuromorphic Asynchronous Event-Based Cameras. *Neural Computation* **27**(4), 925–953 (04 2015). https://doi.org/10.1162/NECO_a_00720, https://doi.org/10.1162/NECO_a_00720 3
 54. Palmero Cantarino, C., Komogortsev, O.V., Talathi, S.S.: Benefits of temporal information for appearance-based gaze estimation. In: *ACM Symposium on Eye Tracking Research and Applications. ETRA '20, ACM* (Jun 2020). <https://doi.org/10.1145/3379156.3391376>, <http://dx.doi.org/10.1145/3379156.3391376> 12, 24

55. Posch, C., Serrano-Gotarredona, T., Linares-Barranco, B., Delbruck, T.: Retinomorph event-based vision sensors: Bioinspired cameras with spiking output. *Proceedings of the IEEE* **102**(10), 1470–1484 (2014). <https://doi.org/10.1109/JPROC.2014.2346153> 3
56. Ranjan, R., Mello, S.D., Kautz, J.: Light-weight head pose invariant gaze tracking (2018) 1, 2
57. Rebecq, H., Horstschaefer, T., Scaramuzza, D.: Real-time visual-inertial odometry for event cameras using keyframe-based nonlinear optimization. In: *British Machine Vision Conference* (2017), <https://api.semanticscholar.org/CorpusID:30723444> 3
58. Reverter Valeiras, D., Lagorce, X., Clady, X., Bartolozzi, C., Ieng, S.H., Benosman, R.: An asynchronous neuromorphic event-driven visual part-based shape tracking. *IEEE Transactions on Neural Networks and Learning Systems* **26**(12), 3045–3059 (2015). <https://doi.org/10.1109/TNNLS.2015.2401834> 3
59. Roy, K., Chanda, D.: A robust webcam-based eye gaze estimation system for human-computer interaction. In: *2022 International Conference on Innovations in Science, Engineering and Technology (ICISSET)*. pp. 146–151 (2022). <https://doi.org/10.1109/ICISSET54810.2022.9775896> 2
60. Shen, N., Xu, T., Huang, S., Mu, F., Li, J.: Expert-guided knowledge distillation for semi-supervised vessel segmentation. *IEEE Journal of Biomedical and Health Informatics* **27**(11), 5542–5553 (2023). <https://doi.org/10.1109/JBHI.2023.3312338> 4
61. Shin, W.G., Park, H., Kim, S.P., Sul, S.: Individual differences in gaze-cuing effect are associated with facial emotion recognition and social conformity. *Frontiers in Psychology* **14** (2023). <https://doi.org/10.3389/fpsyg.2023.1219488>, <https://www.frontiersin.org/journals/psychology/articles/10.3389/fpsyg.2023.1219488> 4
62. Sochopoulos, A., Mademlis, I., Charalampakis, E., Papadopoulos, S., Pitas, I.: Deep reinforcement learning with semi-expert distillation for autonomous uav cinematography. In: *2023 IEEE International Conference on Multimedia and Expo (ICME)*. pp. 1325–1330. IEEE Computer Society, Los Alamitos, CA, USA (jul 2023). <https://doi.org/10.1109/ICME55011.2023.00230>, <https://doi.ieeecomputersociety.org/10.1109/ICME55011.2023.00230> 4
63. Song, J., Meng, C., Ermon, S.: Denoising diffusion implicit models. *arXiv preprint arXiv:2010.02502* (2020) 8
64. Tang, C., Wang, X., Huang, J., Jiang, B., Zhu, L., Zhang, J., Wang, Y., Tian, Y.: Revisiting color-event based tracking: A unified network, dataset, and metric. *arXiv preprint arXiv:2211.11010* (2022) 3
65. Tian, Y.L., Kanade, T., Cohn, J.: Dual-state parametric eye tracking. In: *Proceedings of 4th IEEE International Conference on Automatic Face and Gesture Recognition (FG '00)*. pp. 110 – 115 (March 2000) 3
66. Wang, Sung, Venkateswarlu, R.: Eye gaze estimation from a single image of one eye. In: *Proceedings Ninth IEEE International Conference on Computer Vision*. pp. 136–143 vol.1 (2003). <https://doi.org/10.1109/ICCV.2003.1238328> 1
67. Wang, K., Ji, Q.: Real time eye gaze tracking with 3d deformable eye-face model. pp. 1003–1011 (10 2017). <https://doi.org/10.1109/ICCV.2017.114> 3
68. Wang, K., Ji, Q.: 3d gaze estimation without explicit personal calibration. *Pattern Recognition* **79**, 216–227 (2018). <https://doi.org/https://doi.org/10.1016/j.patcog.2018.01.031>, <https://www.sciencedirect.com/science/article/pii/S0031320318300438> 23
69. Wang, X., Li, J., Zhu, L., Zhang, Z., Chen, Z., Li, X., Wang, Y., Tian, Y., Wu, F.: Visevent: Reliable object tracking via collaboration of frame and event flows. *IEEE Transactions on Cybernetics* (2023) 3

70. Weikersdorfer, D., Adrian, D., Cremers, D., Conradt, J.: Event-based 3d slam with a depth-augmented dynamic vision sensor (06 2014). <https://doi.org/10.1109/ICRA.2014.6906882> 3
71. Wood, E., Bulling, A.: Eyetab: Model-based gaze estimation on unmodified tablet computers. In: Proceedings of the Symposium on Eye Tracking Research and Applications. p. 207–210. ETRA '14, Association for Computing Machinery, New York, NY, USA (2014). <https://doi.org/10.1145/2578153.2578185>, <https://doi.org/10.1145/2578153.2578185> 1
72. Xiang, L., Ding, G., Han, J.: Learning from multiple experts: Self-paced knowledge distillation for long-tailed classification (2020) 4
73. Young, L.R., Sheena, D.: Survey of eye movement recording methods. Behavior research methods & instrumentation 7(5), 397–429 (1975) 3
74. Zhao, G., Yang, Y., Liu, J., Chen, N., Shen, Y., Wen, H., Lan, G.: EV-eye: Rethinking high-frequency eye tracking through the lenses of event cameras. In: Thirty-seventh Conference on Neural Information Processing Systems Datasets and Benchmarks Track (2023), <https://openreview.net/forum?id=bmfMNI1bU> 4
75. Zhu, Z., Ji, Q., Bennett, K.: Nonlinear eye gaze mapping function estimation via support vector regression. In: 18th International Conference on Pattern Recognition (ICPR'06). vol. 1, pp. 1132–1135 (2006). <https://doi.org/10.1109/ICPR.2006.864> 1, 12, 24
76. Zhu, Z., Hou, J., Lyu, X.: Learning graph-embedded key-event back-tracing for object tracking in event clouds. Advances in Neural Information Processing Systems 35, 7462–7476 (2022) 3
77. Zhu, Z., Hou, J., Wu, D.O.: Cross-modal orthogonal high-rank augmentation for rgb-event transformer-trackers. In: Proceedings of the IEEE/CVF International Conference on Computer Vision. pp. 22045–22055 (2023) 3

(Supplementary Material)

In the supplementary material, we provide a thorough examination of the dataset in Sec. S1. Additionally, Sec. S2 offers a comprehensive elucidation of our gaze tracker’s training objectives. Furthermore, an in-depth rationale for the settings of the diffusion denoiser is presented in Sec. S3. Lastly, we present further experiments on the continuous estimation of gaze locations in Sec. S4. *Note that we have also submitted the code and a demo video.*

S1 Dataset

We utilized a hybrid Event IR-based near-eye gaze tracking dataset [2] to assess the performance characteristics of our novel gaze estimation framework. The dataset integrates a sophisticated DVAIS346b sensor (iniVation) with a high-resolution 25 mm f/1.4 VIS-NIR C-mount lens (EO-#67-715), further augmented with a UV/VIS cut-off filter (EO-#89-834) to capture the ocular dynamics of subjects securely positioned using an ophthalmic headrest coupled with restraining apparatus to minimize potential head movement artifacts. Congruent timestamp alignment ensures temporal synchronization of the sensors, facilitating the concurrent acquisition of 346×260 px greyscale frames and the corresponding event data. Visual stimuli are rendered on a 40-inch diagonal, 1920×1080 px display (Sceptre 1080p X415BV-FSR), strategically situated at a standard reading distance of 40 cm from the participants. The spatial configuration of the display ensures its horizontal centrality and vertical orientation such that a user’s direct gaze converges approximately at a locus positioned at one-third from the upper boundary of the screen, thereby simulating a naturalistic viewing angle.

The dataset encompasses biometric recordings from 24 subjects, partitioned into two distinct experimental conditions tailored to elicit different oculomotor responses: stochastic saccadic movements and controlled smooth pursuit tracking. The visual stimulus, a 40×40 px luminous green fixation cross, is superimposed on a circular background with a diameter of 20 px, set against a uniform black field to minimize peripheral visual cues. The display apparatus is configured to encompass a visual field of view (FoV) of $64^\circ \times 96^\circ$.

During the first experimental paradigm, subjects were instructed to direct their gaze towards the stimulus, which materialized at random within a grid matrix of 121 discrete points (an 11×11 grid pattern projected onto the display medium), with each point being presented for a temporal duration of 1.5 seconds. This sequence of locations was uniformly randomized and remained consistent across all participants.

In the subsequent experimental paradigm, the subjects’ task was to maintain visual fixation on the stimulus as it traversed a predefined square-wave trajectory. This trajectory commenced at the upper boundary of the display and proceeded in a downward motion, simultaneously covering the full horizontal extent of the screen, with a vertical displacement amplitude of 150 px. Despite the intentional induction of saccadic jumps and smooth pursuit movements within the experimental framework, the resulting dataset encapsu-

lates a plethora of involuntary eye dynamics, including microsaccades and ocular tremor, thereby offering a comprehensive profile of ocular motion behavior.

S2 Training Objective

We train our two-stage gaze estimation framework in a two-stage training manner. In the first stage, we deploy the standard cross-entropy loss function, denoted as \mathcal{L}_e , to guide the local experts training, which ensures that our local experts maintain optimal performance. We distill these local experts into a student network in the second stage. Noted that in the second training stage, we add more substantial supervision for the entire dataset training, allowing our network to learn better. The the standard cross-entropy loss function is also kept to ensure stable performance as hard loss. Meanwhile, we use the attention metrics of local experts and apply the Kullback-Leibler Divergence loss function, denoted as a soft loss \mathcal{L}_s , to guide the learning of the student network. Finally, a Mean Squared Error loss function, denoted as a feature map loss \mathcal{L}_d , is used to distill the local experts better. The loss of the whole model is the weighting of these three losses:

$$\mathcal{L}_e = \mathcal{L}_{CE}(\hat{\mathbf{Y}}, \mathbf{Y}) \quad (\text{S7})$$

$$\mathcal{L}_s = \mathcal{KL}(\mathbf{ATN}_S, \mathbf{ATN}_E) \quad (\text{S8})$$

$$\mathcal{L}_d(x, x_i) = \left\| x - \frac{x_i}{\sqrt{\bar{\alpha}_i}} \right\|_2^2 = \left\| x - x_0 + \sqrt{\frac{1 - \bar{\alpha}_i}{\bar{\alpha}_i}} \epsilon' \right\|_2^2, \quad (\text{S9})$$

$$\mathcal{L} = \alpha \cdot \mathcal{L}_e + \beta \cdot \mathcal{L}_s + \gamma \cdot \mathcal{L}_d \quad (\text{S10})$$

where \mathcal{L}_{CE} indicates the cross-entropy loss, $\hat{\mathbf{Y}} \in \mathbb{R}^L$ and $\mathbf{Y} \in \mathbb{R}^L$ represent the predicted and ground-truth locations, \mathcal{KL} indicates the KL-divergence, and $\mathbf{ATN}_S, \mathbf{ATN}_E \in \mathbb{R}^{H \times W}$ show the attention matrices. Moreover, \mathcal{L}_d is shown in the Eq. 4 in the manuscript, and α , β , and γ are corresponding weight for balancing different loss terms. Drawing conclusions from our extensive ablation experiments, we set α , β , and γ as 1, 1, and 500, respectively.

S3 Training of Diffusion Denoiser

During the training process, we optimize the diffusion denoiser with following loss term

$$L_{Diff} = \nabla_{\theta} \left\| \sum \delta \right\|^2 + \left\| \sigma(\delta) - \sqrt{2} \right\|^2, \quad (\text{S11})$$

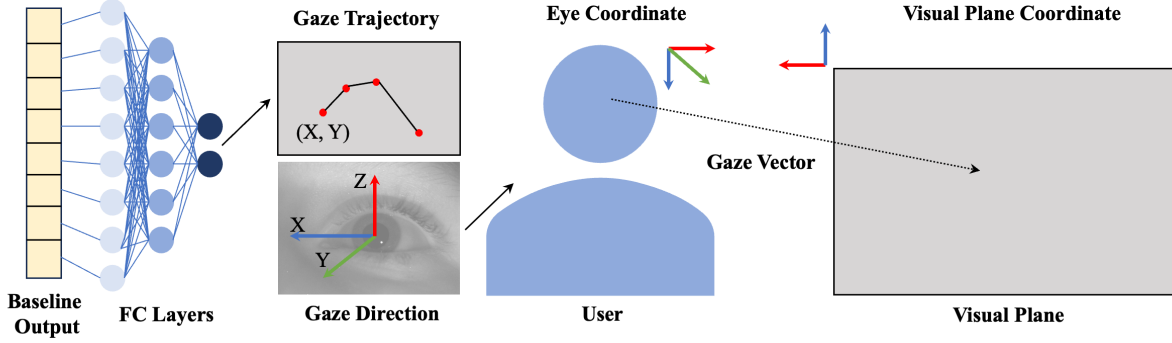


Fig. S8: Integration of a continuous location prediction network for eye tracking within a pre-trained model via fully connected layer units.

Here, we give the detailed explanation of it. Since $\epsilon \sim \mathcal{N}(\bar{\epsilon}; 0, 1)$ and we expect $\epsilon_{\theta}(\sqrt{\frac{\bar{\alpha}_t}{\bar{\alpha}_i}}x_i + \sqrt{1 - \frac{\bar{\alpha}_t}{\bar{\alpha}_i}}\epsilon, t) \sim \mathcal{N}(\bar{\epsilon}; 0, 1)$ Thus, for δ

$$\delta = \epsilon - \epsilon_{\theta}(\sqrt{\frac{\bar{\alpha}_t}{\bar{\alpha}_i}}x_i + \sqrt{1 - \frac{\bar{\alpha}_t}{\bar{\alpha}_i}}\epsilon, t), \quad (\text{S12})$$

it should follow $\delta \in \mathcal{N}(0, 1) - \mathcal{N}(0, 1) = \mathcal{N}(0, \sqrt{2})$. Then we regularize $\sum \delta \rightarrow 0$ and $\sigma(\delta) \rightarrow \sqrt{2}$, which is exact the training objective Eq. S11.

S4 Aligning Continuous Location Prediction into Pre-trained Model

An essential requirement of eye tracking technology is the capability to dynamically estimate the point of gaze. After distillation of local experts into a comprehensive model, our system can provide a rough estimate of the gaze locus with low resolution. Building upon the foundation of a pre-trained model, we generate accurate three-dimensional coordinates for the free gaze point [19, 45, 68]. To produce the actual location of the gaze intersection with the screen, we have designed a branch for gaze projection coordinates, as depicted in the Fig. S8. Specifically, we have adapted the final output layer, traditionally responsible for generating class labels, to directly predict the two-dimensional coordinates of the gaze point on the screen [21, 44]. Concurrently, we refined the optimization objective of the model by transitioning to an alternative loss function, designated as \mathcal{L}_c , for the fine-tuning of the pre-trained model parameters. The MSE loss function was selected to direct the training process of the gaze position regression model, providing a robust quantitative measure for minimizing the discrepancy between the predicted and actual gaze coordinates. This strategic modification is predicated on enhancing the model’s precision in capturing the subtleties of gaze behavior.

$$\mathcal{L}_c = \|\hat{\mathbf{P}} - \mathbf{P}\|_2^2 \quad (\text{S13})$$

where $\hat{\mathbf{P}} \in \mathbb{R}^2$ and $\mathbf{P} \in \mathbb{R}^2$ represent the predicted value of the model and the ground-truth value of the gaze point, respectively.

Table S4: Quantitative results of our methods of continuous location prediction. \downarrow indicates the smaller, the better.

Method	S-T GE [54]	Dilated-Net [8]	EventGT [75]	HE-Tracker [7]	Ours
MAE \downarrow	6.980°	3.589°	3.900°	3.655°	3.184°

This modification enables the system to translate the abstract understanding of where a person is looking into a concrete set of screen coordinates, facilitating applications that require precise tracking of the user’s point of gaze. After that, our system establishes a spatial coordinate system with the human eye as the origin in three-dimensional space. Subsequently, using randomly captured near-eye RGB and event data, our system outputs continuous location predictions. The quantitative results of this assessment are systematically presented in Table S4.